Design of a dynamic tribometer applied to piezoelectric Inertia Drive Motors

- In situ exploration of stick-slip principle -

Fabien Dubois[1,2)*], Christian Belly[1)], Aurélien Saulot[2)] and Yves Berthier[2)]

1) Cedrat Technologies S.A.,

59 chemin du vieux chêne, Innovallée, 38246 Meylan Cedex, France

2) Laboratory of Mechanical Contacts and Structures, Université de Lyon, CNRS, INSA-Lyon, LaMCoS UMR5259,

F-69621 Villeurbanne, France

*Corresponding author: fabien.dubois@insa-lyon.fr

Abstract

In Inertia Drive Motors, generated motion is based on stick-slip principle. Current analytical models are predictive enough to calculate qualitatively their optimal performances, such as maximal step size and speed, with relatively few input parameters. But, they do not take into account the contact life and temporal evolution of parameters as friction factor all along lifetime of IDM. So, analytical models reach their limits when precise predictions are necessary. This investigation aims at understand wear mechanisms to model temporal evolution of friction. Such an understanding requires the reconstitution of the contact life through the evaluation of 1st and 3rd body flows. To do so, a new IDM-representative tribometer is designed. First bodies - coated TA6V and polymer - are not see-through. They are replaced alternatively by an intermediate transparent first body to observe the contact dynamically and *in-situ*. Friction factor, step size and mean speed are also measured. Preliminary results shows that wear profiles from real IDM and tribometer are similar. Direct observations bring out particles of TA6V coating are firstly snatched, then moves in contact and finally trigs others particle detachments.

Keywords: stick-slip instabilities, dynamic in situ visualization, contact mechanic, 3rd body behavior

1. Introduction

Piezoelectricity is a property of some materials to convert mechanical energy into electrical energy. This phenomenon, called direct effect, has been discovered in 1880 by Pierre and Jacques Curie [1]. Piezoelectric elements are used since such sensors including strain gauges. Main point of piezoelectricity is its reversibility, called inverse effect, and discovered in 1881 by Gabriel Lippmann [2]. When electrical energy is supplied to piezoelectric elements, they convert it into a micrometric displacement. By neglecting the hysteresis of piezoelectric element [3], it becomes possible to work out a displacement-voltage proportional actuator. In 1987, Pohl [4] uses the inverse effect to introduce the concept of Stepping Piezoelectric Inertia Drive Motors (IDM) for a scanning tunneling microscope application. A piezoelectric ceramic is attached to an oscillating mass: first friction 1st body [5] (Fig. 1.a, b). This first body is set in contact with a moving mass: second 1st body. Successively, ceramic slow contracts - stick phase: the first bodies move together of a few micrometers. Then, it fast expand - slip phase: the first body No. 1 reaches its original position whereas the first body No. 2 remains in its new position (Fig. 1.b). Direction of movement is reversible when expand is slow and contract is fast. Friction is no more synonym of energy loss but becomes a relay in motion

transmission. Mastering it aims at controlling movement and energy dissipation into the contact. IDM have then evolved these last thirty years [6, 7, 8] to branch out into many industrial sectors such as optronic [9] and medical applications [10]. These motors are useful in embedded applications where celerity, force and volume are low (respectively a few centimeters per second, a few newtons and lower than 15 cubic centimeters) and when micrometric resolution positioning is necessary [11].

Depending on application, specific constraints, such as no wear generation or biocompatibility, must be respected. Here, biocompatibility [12, 13] and wear are bound by the tribological circuit [14]. System configuration was decided to set the first body that wears the most in macroscopic moves to avoid excessive wear particle deposit leading to dysfunction (Fig. 1.c).

This investigation focuses on the understanding of this wear mechanism through the evaluation of 1st and 3rd body flows to get the overall understanding of the tribological system. It is based on Linear Stepping Piezo Actuator (LSPA, Fig. 2) from Cedrat Technologies company [15].

An analytical LuGre model of macroscopic friction has been introduced in [16]. Although qualitative prediction is good to calculate optimal performances, a time representative limitation has been identified. Friction coefficient is used as an input static parameter without taking into account wear of the interfaces. A new tribometer is introduced to raise that limit.

Dynamic and *in-situ* observations give an overview of what happens in contact, and so reconstitute the associated tribological circuit, by replacing successively 1st bodies with transparent ones. The comparison between measurements and observations led to a better understanding of the 3rd behavior in IDM. This investigation is completed by a discussion about the use of an intermediate transparent 1st body and its impact on the analysis.

2. Material and methods

2.1. Studied IDM: LSPA30µXS

Linear Stepping Piezoelectric Actuators (LSPA) are composed of an Amplified Piezoelectric Actuator (APA®) [15] with a shaft, first 1st body, and a clamp, second 1st body. TA6V-polymer rubbing couple is used in LSPA-30µXS design (Fig. 2). Geometry of shaft is rectangular. Material is non disclosed polymer. Clamp interface is four convex half cylinders. Preload is provided by a spring whose stiffness is 2.5kN/m. Mean Hertz contact pressure is 4.2MPa.

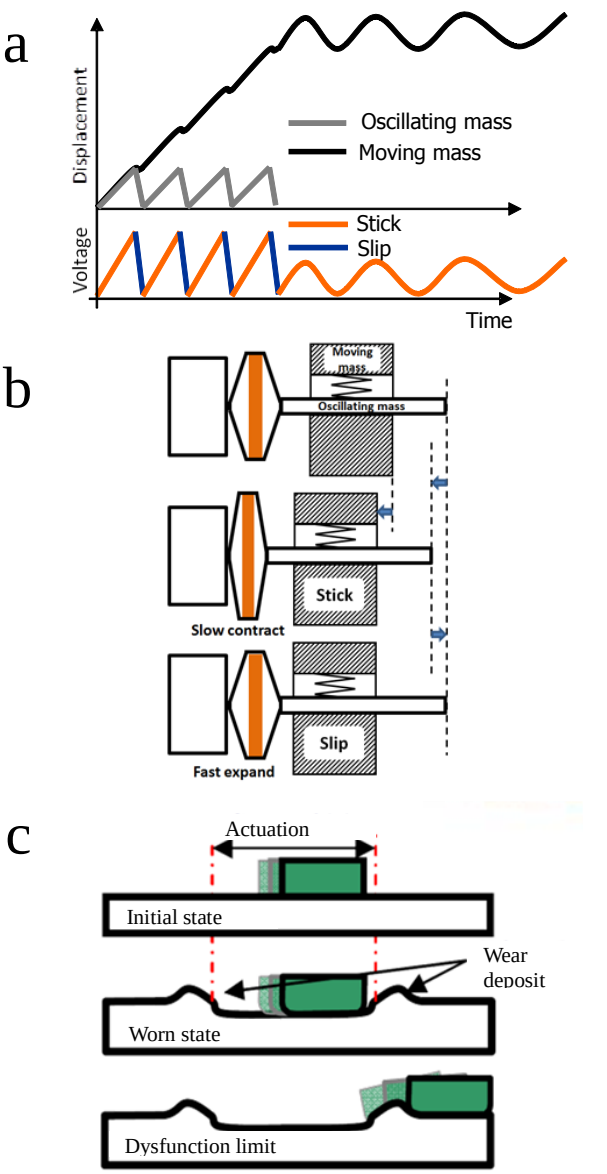

Fig. 1. IDM principle: (a) Proportionality between voltage order and piezoelectric microscopic displacement. (b) Microscopic to macroscopic displacement by stick-slip steps sequence. (c) Wear mechanism when polymer makes macroscopic moves along TA6V stroke.

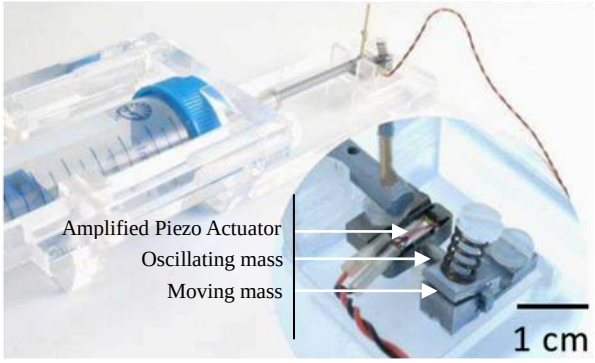

Fig. 2: Cedrat Technologies IDM. LSPA30µXS, oscillating shaft first 1st body is in polymer and mobile clamp second 1st body is in coated TA6V.

2.2. Contact life: A new dynamic *in-situ* IDM tribometer

2.2.1 Tribometer design constraints

Through the 3rd body concept, first constraint is to link friction factor evolution to direct observations. Purpose is to understand the life contact with a mechanical approach and being able to attribute accommodation sites and modes [14]. Current first bodies are not see-through. First, friction factor with coated TA6V against polymer is measured. Then, first bodies are alternatively replaced by transparent one to see through. By finally comparing direct *in-situ* observations, microscopy analyses and measurements, it becomes possible to get sought tribological circuit. Design of the tribometer must provide an oscillating shaft with a hole and space to glue – like in a real IDM – rubbing samples.

Second challenge was to find an optimal size of the tribometer, allowing performing all the measurements at the same time while remaining at IDM scale. The main point was to maintain a representative 3rd body life inside the contact. If the tribometer is too large, global speed would decrease and local 3rd body behavior would change. It the tribometer is too small, there is not space enough to set all the sensors. Therefore, mass and volume of the bench has been optimized to keep same orders of magnitude than LSPA: actuation force (2N), speed (10mm/s), contact pressure (10MPa) and actuation frequency (1kHz). Contact has also been simplified. Instead of four - LSPA30µXS configuration-, clamp and shaft has been replaced by a pin on pad contact (Fig. 3) whose geometry is that of LSPA30µXS – cylinder/flat contact. Spring preload has been kept with a 2.5kN/m stiffness order of magnitude.

Finally, guiding must be considered to ensure linear movement without dissipating too much energy. New Way air guiding has been chosen for their normal stiffness – 4N/µm - and their friction factor is neglegible because there is no contact with moving mass (Fig. 3). Three 12mm x 24mm flat rectangular air guiding (Fig. 5.g) are integrated in dovetail to both ensure guiding, lift and limiting the number of air input.

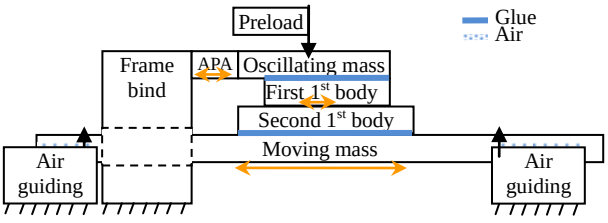

Fig. 3: Principle scheme of tribometer. 1st bodies are bound to the moving and oscillating mass by the same glue as that real IDM. Guiding is provided by are air to minimize parasitic friction and only studying friction between 1st bodies. Preload is provided by a spring like in real IDM. Double arrows: APA generates small amplitude dissymmetric oscillations. First 1st body relays and converts these small oscillations in macroscopic movement through stick-slip principle.

2.2.2 Tribometer instrumentation

All measurements and associated sensors are listed in Table 1 and illustrated (Fig. 4.a). National Instrument USB-6259 BNC electronic board (Fig. 4.b) associated with Labview (Fig. 4.c) is used to generate actuation signal and acquire measurement data.

Piezoelectric ceramic can be compared to electrical capacitance. Current consumption depends on voltage and frequency of actuation signal. If current limitation of power supply is two low (<471mA for a 2kHz and 150V actuation signal here), mechanical performances are decreased. Linear amplifier (Cedrat Technologies LA75C) (Fig. 4.d) is used with 2.4 ampere current limitation. Voltage and current (Fig. 4.e,f) are measured to control power supply.

Since actuation frequency is 1kHz to keep same order of magnitude with LSPA, common camera are not relevant for direct observations, high speed camera is used instead. A Vision Research V710 high-speed camera (Fig. 4.g) associated with PCC2.6 software (Fig. 4.h) is used with 5kHz frame per second, associated with a Navitar 6000 optical zoom to focus on the contact and a Schott KL2500 Led (Fig. 4.i) to provide enough light without harming contact. Observation window is 8 mm x 5 mm with 360 x 480 pixels. Each pixel measures 15µm by side. Step size is 75µm so there are 5 pixels by step.

Table 1 List of integrated measurement in test bench

Measures	Sensors
Friction factor:	
- Normal force	Strain gauge
- Tangential force	Optical sensors+processing
Direct observations:	
- *In-situ*	Camera through lenses
- Macroscopic friction	Fast camera
Linear momentum:	
- Before friction	Differential laser-
- After friction	-vibrometer sensor
Initial & Final conditions	Microscope/SEM-EDX

To complete analysis of the friction interface (Fig. 5.a), a test body has been designed [17] to measure normal force in a [3N; 9N] range with a HBM strain gauge - 2 half-bridges (one on each side of the test body) referenced 1-DA53K3.2 / 350_E (Fig. 5.b). Normal stiffness is 41.2kN/m. Tangential force and relative displacement of oscillating mass and moving mass are measured with Numerik Jena optical sensors (Fig. 5.e-f). Characteristics are a 3 millimeters stroke, 0.1µm resolution and 30 kHz sampling.

Mechanical representativity of the contact is finally controlled by the spring preload, like in real IDM with a global normal stiffness of 2.3kN/m in the normal

direction which is closed to the IDM stiffness - 2.5kN/m.

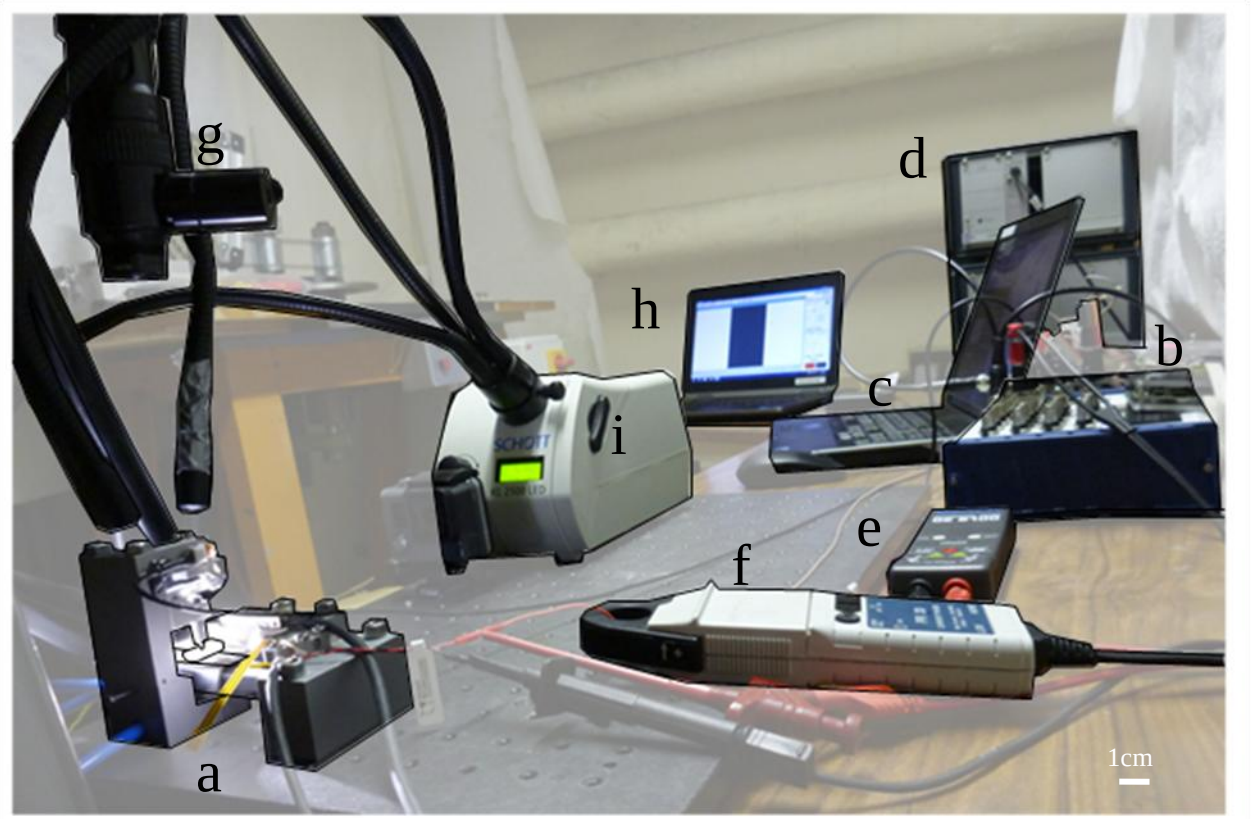

Fig. 4: Global SPA-tribometer setup. (a) Tribometer setup. (b) Schott KL 2500 LED. (c) Current probe to get input electrical energy. (d) Voltage probe to get input electrical energy. (e) National Instrument NI USB-6259 BNC acquisition and generation card. (f) LA75C Cedrat Technologies power supply and SG75 strain gauge controller. (g) Labview computer manage signals and post-treatment. (h) V710 Vision Research high speed camera and Navitar6000 optical zoom. (i) Fast camera computer.

2.3. 3rd body approach

Godet and Berthier proposed a phenomenological concept from experimental observations called the tribological triplet [5]. When two first bodies are in contact and in relative motion, an interfacial layer creates - called 3rd body - which is subjected to speed gradient. Such 3rd body flows inside the contact [18]. Wear is approach in term of 3rd body flow. The different flows are illustrated in (Fig. 6). Q_s^i is internal source of 3rd body, got by particle detachment from 1st bodies. Q_s^e is external source got by environment particle detachment. Q_i is internal flow of particle inside the contact. Q_e is ejection flow divided in Q_r and Q_w. Q_r is recirculation flow when particle left the contact and are introduced again then. Q_w is wear flow for particles leaving definitively the contact.

3rd body causes the activation of the different flow rates in the tribological system. Highlighting it is essential to control lifetime of IDM.

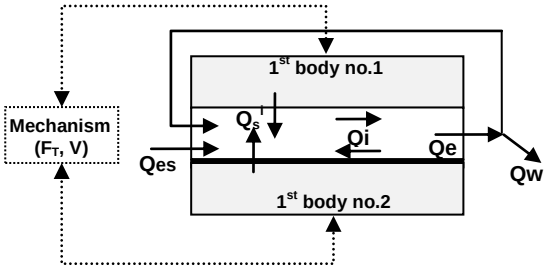

Fig. 5: Tribological circuit principle scheme for Coated TA6V pad against glass pin.

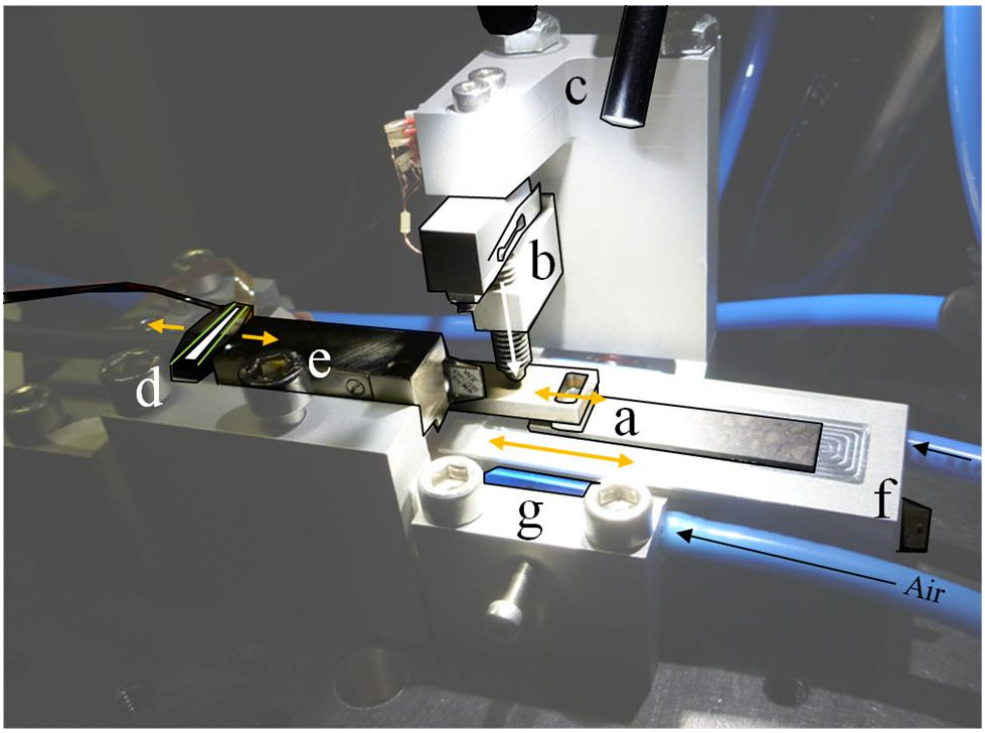

Fig. 6: Tribometer setup. (a) 1st bodies contact. Current geometry is semi-circular pad on pad. (b) Preload function (write arrow) is provided by a spring contained in a screw. Applied force is proportional to screw position and measured by a strain gauge mounted on specific deformable test body. Applied Normal force range is [3N; 10N]. (c) Extra light is provided by Schott® KL 2500 LED to make fast camera acquisition possible without harming contact. (d) Piezoelectric actuator linked to oscillating mass. Strain gauge is mounted on actuator to get actuation force. (e) Numerik Jena® optical sensor to get displacement, speed and acceleration of oscillating mass. Sampling is 30kHz, resolution is 0,1µm. (f) Numerik Jena® optical sensor to get displacement, speed and acceleration of moving mass. Sampling is 30kHz, resolution is 0,05µm. (Only scale tape is seen into the moving mass) (g) Guiding and lift are provided by New way® air bearings.

3. Measurements : tribometer high speed observations

A Labview program has been used to generate thousand back and forth of three steps. Each step lasts 2ms – 1ms for actuation signal and 1ms of deadtime to damp free oscillations - so total acquisition lasts 12 seconds. High speed camera is set to 5000 frame per second (fps). It is compromised between getting a lot of frames per actuation period and light power. More fps means less aperture time (0.1ms currently) so less visibility to observe the contact.

Tests are divided in three phases, one per material couple: Coated TA6V / Polymer, Glass / Polymer and Glass / Coated TA6V. In each phase, five sessions of actuations are performed which leads to five thousands back and forth. Observations on both glass/polymer and glass/coated TA6V are used to reconstitute polymer/coated TA6V wear mechanisms.

3.1. Glass pin / Polymer pad

All along the five thousands back and forth, no flow is visibly activated (Fig. 7.a).

3.2. Glass pin / TA6V pad

From the first thousand cycles, dark particles appear (Fig. 7.b). Then, these particles move in actuation direction until the end of the test. Black spot appears on glass pin and a bright track full of particles remains on the pad after the contact. Around 3500 cycles moves perpendicularly to the actuation direction and trigs occurrence of a new wear track in the actuation direction.

Around two thousand cycles, edges of real contact appears. Particle deposit along these edges increases permanently until the end of the test.

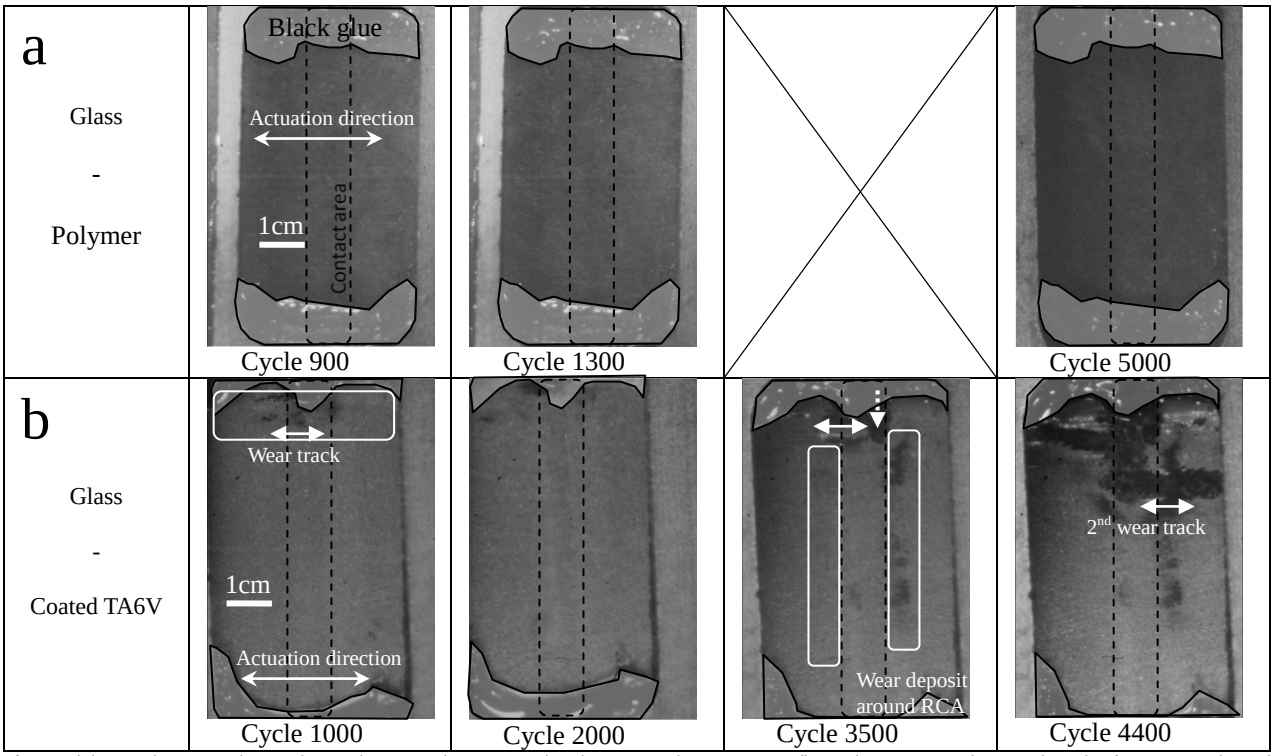

Fig. 7: High speed camera observations. Glass on polymer actuation does not make appear any flow. Glass on coated TA6V trigs Qis after 1000 cycles. Qi is activated after 2000 cycles and deposit appears around real contact area. After 3500 cycles, Qe, Qes and Qw are activated. After 4400 cycles, 3rd body particle generate a second track.

4. Results

4.1. Tribometer representativity

By design, mass of oscillating part and moving part are respectively 12gr and 34gr. Friction factor has been measured with polymer against coated TA6V before tests: 0.41+/-0.04. Preload has been set to 5N. Mean Hertz contact pressure is 6.9MPa which closed to LSPA reality. These parameters are used as input data in Simulink modeling used to describe real IDM behavior. Steps are measured and plotted in (Fig. 8). Error on displacement step size is 8.4% which relevant enough to confirm macroscopic representativity of the tribometer.

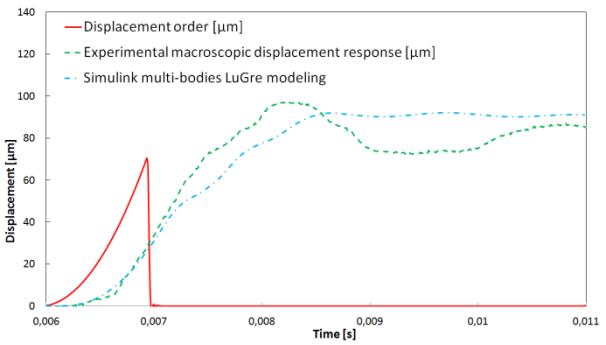

Fig. 8: Comparison between experimental measurements and Simulink analytical modeling before tests. Experimental step size is 90µm and modeled step size is 83µm.

After tests, first bodies are observed with optical microscopy (Fig. 9). In real IDM (Fig. 9.a) like in tribometer (Fig. 9.b), when polymer rubs against coated TA6V, wear profiles are similar. Fibers of the polymer are broken and scattered in the wear track. Coating is snatched from the contact area and moved to its frontier. Tribometer is representative of a real IDM at the scale of contact.

4.2. Wear mechanism

When glass is actuated against polymer, none flow is visibly activated at this scale of observation (Fig. 7.a) and no macroscopic wear appears (Fig. 9.d). In case of glass against coated TA6V, for the thousand first cycles (Fig. 7.b), black particles detachment is supposed to be that of coating because glass is transparent. These particles are trapped in glass and wear track appears on it in actuation direction (Fig. 9.c). Q_s^i from coating is activated. Then Q_i is activated with 3rd body particles newly generated. Particles stick both interfaces and moves with contact in actuation direction. Wear track has same aspect as TA6V pad without coating so it is presumed to be 1st body. Emergence of the real contact area lasts longer. After five thousands cycles, actuation track on pin is as bright as pin without coating but there is no deposit outside (Q_w is not activated) so particles remained in contact.

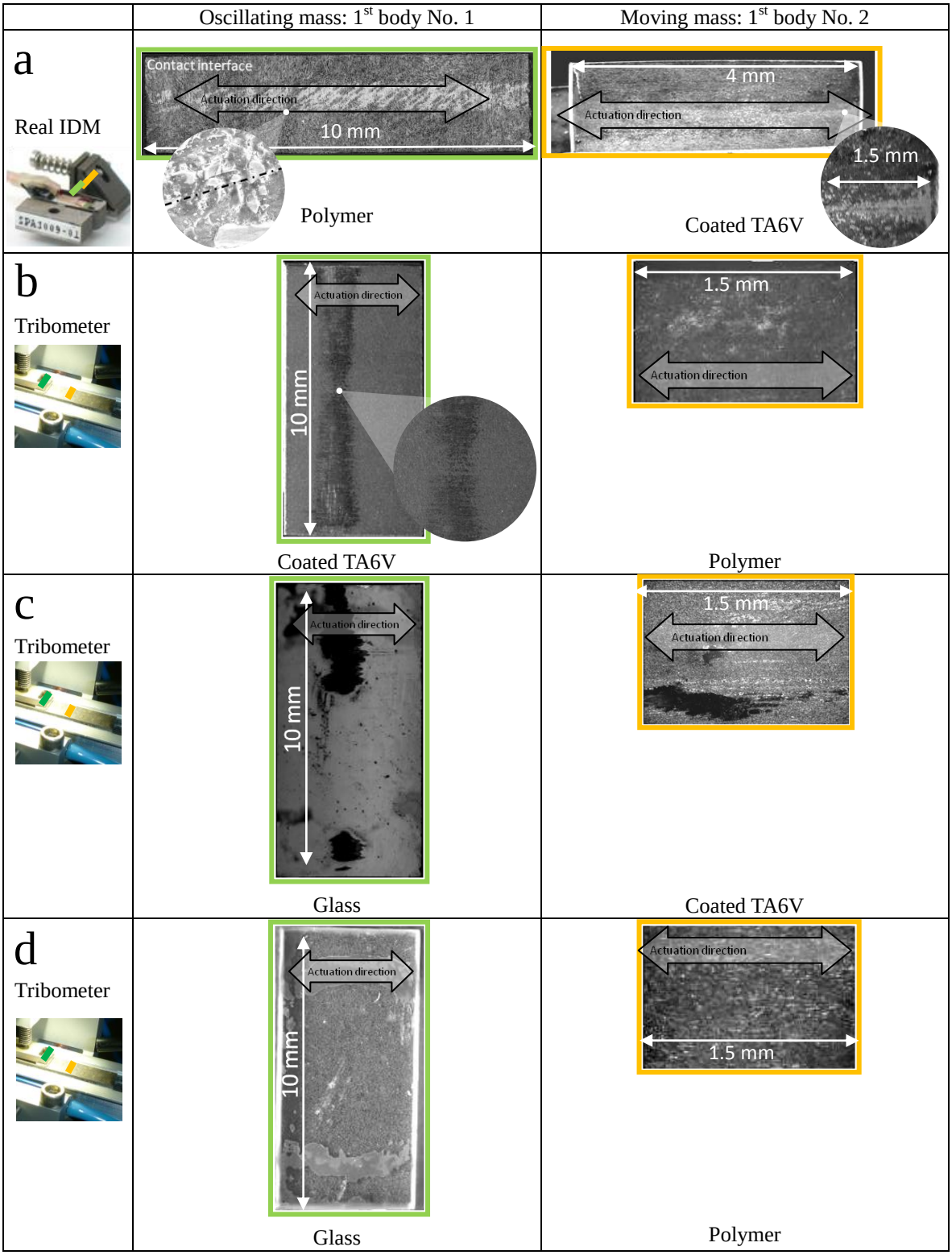

Fig. 9: Wear profile comparison after 5000 cycles. (a) Real IDM. On the polymer side, black matrix of the polymer is brighter in wear track. Zoom shows many little bright fibers in track and a few bigger fibers outside the track. On the coated TA6V side, 1st body appears under coating in wear track and a deposit of dark particles surrounds it. (b) Tribometer - real rubbing couple. Coated TA6V and polymer wear profiles are similar as in real IDM. (c) Tribometer - glass/coated TA6V. Particles of coating are trapped in pin. Wear track in actuation direction appears on these particles only. (d) Tribometer – glass/polymer. Neither glass nor polymer is worn.

From these preliminary observations, wear mechanism into coated TA6V pin against polymer is deduced. Coating is quickly snatched from TA6V 1st body and moves in the actuation direction. Lift and speed accommodation are no more located in screen interfaces but in 3rd body. By actuation, some of the particles moves seemed to agglomerate. Then, they move with contact and snatch other particles. These particles crush fibers of polymer in smaller fibers. Some others, more pulverulent, remains in the wear track and are reintroduced when pin go on again. In case of glass against polymer, nothing happened. So polymer is not source of flow activation but coating is.

5. Conclusion

Using an intermediate sample made possible a direct *in-situ* analysis but this point must be discussed. Chosen material of intermediate body is glass because silicon oxide is in the chemical composition of the polymer and coating. Optical properties made possible direct observations. Parts were geometrically designed as a function of material properties to respect same contact pressure. Roughness is as low as possible to not disrupt optical signal. Resulting direct observations, consistent with real IDM wear profiles, have validated the use of these intermediates parts. Thus, tribometer tribological realism is validated.

Preliminary results are encouraging. As expected, macroscopic step size and wear profiles were similar between analytical modeling, real IDM behavior and tribometer behavior.

Observations show how wear mechanism is activated in case of coated TA6V against polymer. In first case, coating particles are quickly detached from TA6V pin. Then, theses particles snatch other ones on the pin side, and crush fibers on the pad side. Now the representativity of the tribometer is demonstrated, mechanism that trigs the first detachment must be understood. It means including the accommodation modes [18] in the investigation. These observations will be confirmed by a wider test campaign and chemical analysis trough Scanning Electron Microscopy associated with energy dispersive X-ray spectroscopy. Furthermore, FEM model of the tribometer will be worked out to give access to the stress distribution near and far away from the contact and to link it with previous observations.

6. References

[1] Curie, J. and Curie, P., “Development, by pressure, of polar electricity in hemiedric crystals with inclined faces,” Journal de Physique Théorique et Appliquée, 91, 1880, 294–295 (in French).

[2] Lippmann, G., “Principle of electricity conservation, or second principle of electrical phenomena theory,” Journal de Physique Théorique et Appliquée, 10, 1, 1881, 381–394 (in French).

[3] Breguet, J. M., “Actuators "stick and slip" for micro-manipulators,” PhD thesis, EPFL, 1998 (in French).

[4] Pohl, D. W., “Sawtooth nanometer slider: A versatile low voltage piezoelectric translation device,” Surface Science, 181, 1-2, 1987, 174–175.

[5] Godet, M., “The third-body approach: A mechanical view of wear,” Wear, 100, 1-3, 1984, 437–452.

[6] Morita, T., “Miniature piezoelectric motors,” Sensors and Actuators A: Physical, 103, 3, 2003, 291–300.

[7] Belly, C., Bagot, M., and Claeyssen, F., “High resolution actuators for severe environments,” Proc. Precision Assembly Technologies and Systems, Chamonix, France, 371, 2012, 89–96.

[8] Belly, C., Buttery, M., and Claeyssen, F., “Thermal vacuum behaviour of a stepping piezo actuator,” Proc European space mechanisms and tribology symposium, Constance, Germany, 653, 23, 2011, 195-199.

[9] Belly, C., Porchez, T., Dubois, F., and Barillot, F., “Long stroke/high resolution tip tilt mechanism,” In Proc Actuator, Bremen, Germany, 2014.

[10] Khalaji, I., Hadavand, M., Asadian, A., Patel, R. V., and Naish, M. D., “Analysis of needle-tissue friction during vibration-assisted needle insertion,” In Intelligent Robots and Systems (IROS), Tokyo, Japan, 2013, 4099–4104.

[11] Belly, C., and Charon, W., “Benefits of amplification in an inertial stepping motor,” Mechatronics, 22, 2, 2012, 177–183.

[12] Chinzei, K., Kikinis, R., and Jolesz, F. A., “MR compatibility of mechatronic devices: design criteria,” In Medical Image Computing and Computer-Assisted Intervention - MICCAI’99, 1679, 1999, 1020–1030.

[13] Von Oldenburg, G., and Speitling, A. D., “Osteosynthetic device of steel, cobalt and/or titanium alloy,” European Patent 1228775 A3, 2002.

[14] Colas, G., Saulot, A., Godeau, C., Michel, Y., and Berthier, Y., “Decrypting third body flows to solve dry lubrication issue - MoS2 case study under ultrahigh vacuum,” Wear, 305, 1-2, 2013, 192–204.

[15]Claeyssen, F., Ducamp, A., Barillot, F., Le Letty, R., Porchez, T., Sosnicki, O., and Belly, C., “Stepping piezoelectric actuators based on APAs,” In Proc Actuator, Bremen, Germany, 2008.

[16] Belly, C., “Inertial piezoelectric motors: designs, achievements, and test applications,” PhD thesis, Université de Technologie de Belfort-Montbeliard, 2011 (in French).

[17] Henein, S., “flexible guiding design,” Presses polytechniques et universitaires romandes, 2001 (in French).

[18] Berthier, Y., “Maurice Godet’s third body”. Tribology series, 31, 1996, 21-30.